

ATMOSPHERE AND SPECTRAL MODELS OF THE *KEPLER*-FIELD PLANETS HAT-P-7b AND TRES-2DAVID S. SPIEGEL<sup>1,2</sup>, ADAM BURROWS<sup>1,2</sup><sup>1</sup>Department of Astrophysical Sciences, Peyton Hall, Princeton University, Princeton, NJ 08544 and<sup>2</sup>Kavli Institute for Theoretical Physics, UCSB, Santa Barbara, CA 93106-4030*Draft version August 25, 2010*

## ABSTRACT

We develop atmosphere models of two of the three *Kepler*-field planets that were known prior to the start of the *Kepler* mission (HAT-P-7b and TrES-2). We find that published *Kepler* and *Spitzer* data for HAT-P-7b appear to require an extremely hot upper atmosphere on the dayside, with a strong thermal inversion and little day-night redistribution. The *Spitzer* data for TrES-2 suggest a mild thermal inversion with moderate day-night redistribution. We examine the effect of nonequilibrium chemistry on TrES-2 model atmospheres and find that methane levels must be adjusted by extreme amounts in order to cause even mild changes in atmospheric structure and emergent spectra. Our best-fit models to the *Spitzer* data for TrES-2 lead us to predict a low secondary eclipse planet-star flux ratio ( $\lesssim 2 \times 10^{-5}$ ) in the *Kepler* bandpass, which is consistent with what very recent observations have found. Finally, we consider how the *Kepler*-band optical flux from a hot exoplanet depends on the strength of a possible extra optical absorber in the upper atmosphere. We find that the optical flux is not monotonic in optical opacity, and the non-monotonicity is greater for brighter, hotter stars.

*Subject headings:* planetary systems – radiative transfer – stars: individual HAT-P-7, TrES-2

## 1. INTRODUCTION

Extrasolar planets are being discovered at an increasingly rapid pace: roughly a quarter of the currently known exoplanets (numbering more than 450, as of June, 2010) were found since the beginning of 2009.<sup>1</sup> Still, only  $\sim 80$  of the known planets have been seen to transit their parent stars. Transits break the degeneracy between mass and inclination, they allow direct measurement of planetary radii, and they make possible precise measurements of planetary fluxes from secondary eclipse observations. The *Kepler* mission, which is predicted to find many new transiting planets, is, therefore, particularly exciting.

Three transiting planets in the *Kepler* field were identified prior to the beginning of the *Kepler* mission – TrES-2, HAT-P-7b, and HAT-P-11b (occasionally referred to as Kepler-1b, -2b, and -3b). Spiegel et al. (2010) have already published a range of possible atmospheric models of HAT-P-11b; here, we consider HAT-P-7b and TrES-2.

The InfraRed Array Camera (IRAC) instrument on the *Spitzer* Space Telescope has been a boon to exoplanetary science, providing observations that are diagnostic of atmospheric temperature and com-

position for more than a dozen planets. It had four photometric channels, centered at  $3.6 \mu\text{m}$ ,  $4.5 \mu\text{m}$ ,  $5.8 \mu\text{m}$ , and  $8.0 \mu\text{m}$ . Recently, Christiansen et al. (2010) and O'Donovan et al. (2010) used IRAC to measure infrared fluxes from HAT-P-7b and TrES-2, respectively.

HAT-P-7b, discovered by Pál et al. (2008), orbits a large, hot star ( $1.84R_{\odot}$ , spectral type F8). It is one of the most highly irradiated known exoplanets, with a substellar flux of  $\sim 4.8 \times 10^9 \text{ erg cm}^{-2} \text{ s}^{-1}$ . Its orbit is significantly misaligned from the stellar spin vector, indicating a possible third body in the system (Winn et al. 2009; Narita et al. 2009). It is a particularly interesting object in part because *Kepler's* exquisite photometry has allowed measurement of ellipsoidal variations in the star induced by the planet's tidal field (Welsh et al. 2010). TrES-2, by contrast, orbits a nearly solar-type star in a nearly grazing orbit (O'Donovan et al. 2006; Holman et al. 2007; Sozzetti et al. 2007; Raetz et al. 2009). Mislis & Schmitt (2009) find a reduction in transit duration of  $\sim 3$  minutes since 2006, and attribute this shortening to a change in inclination, although analysis by Rabus et al. (2009) does not corroborate such a large change.

The atmosphere modeling strategy that we employ here differs from several others that have been used. Similar to Barman et al. (2005) and Fortney et al. (2006), we calculate radiative equilibrium, chemical equilibrium models. In contrast,

Electronic address: dsp@astro.princeton.edu, burrows@astro.princeton.edu,

<sup>1</sup> See the catalogs at <http://exoplanet.eu> and <http://www.exoplanets.org>.

both Madhusudhan & Seager (2009) and Tinetti et al. (2005, 2007) adjust both chemistry and thermal structure in order to find a best fit to the available data, eschewing equilibrium solutions. This latter method produces chemical and thermal profiles that are not the result of *ab initio* calculations, but that might reveal non-equilibrium behavior. Yet another approach is taken by Showman et al. (2009) and Burrows et al. (2010), who simulate three dimensional structure and dynamics in planetary atmospheres; so far this more sophisticated approach has not produced better fits to observations than the one-dimensional radiative models described above.

Hubeny et al. (2003) were the first to suggest that an extra optical absorber in a hot exoplanet’s upper atmosphere could lead to a thermal inversion. Observations seem to suggest such inversions (Hubeny et al. 2003; Fortney et al. 2006, 2008; Burrows et al. 2007, 2008a; Richardson et al. 2007; Spiegel et al. 2009; Madhusudhan & Seager 2009; Knutson et al. 2008, 2010), and the strong optical absorber titanium oxide (TiO) has frequently been suggested as the possible culprit responsible for the inferred inversions. However, in the absence of strong mixing processes, the molecular weight of TiO would tend to make it settle to the bottom of the atmosphere. Furthermore, cold traps on the nightside and below the hot upper atmosphere on the dayside can cause TiO to condense into solid grains, which necessitates even stronger macroscopic mixing to keep TiO aloft in the radiatively important upper atmosphere. Since the photospheres are above the radiative-convective boundaries, they are stably stratified; it is not obvious whether such strong mixing obtains in such a stable region (Spiegel et al. 2009). Various authors have tried to estimate the amount of macroscopic mixing and have found that, in some regions of the day-side atmosphere, the mixing might be vigorous enough to maintain TiO at altitude (Showman et al. 2009; Li & Goodman 2010; Madhusudhan & Seager 2010), though Youdin & Mitchell (2010) point out that turbulent diffusivity in excess of  $10^7 \text{ cm}^2 \text{ s}^{-1}$  might lead to overinflation of some planets through downward transport of entropy. Zahnle et al. (2009) suggest that sulfur photochemistry provides another avenue for achieving the additional upper-atmosphere optical opacity that is needed to produce hot upper atmospheres and inversions. Knutson et al. (2010) find that the presence of thermal inversions appears to be inversely related to the host stars’ ultraviolet (UV) activity, raising the possibility that strong incident UV destroys molecules that may be responsible for thermal inversions. Here, we remain agnostic on the matter and include, for modeling purposes, an extra source of optical opacity of as-yet unknown origin.

This paper is structured as follows. In §2, we describe our 1D atmosphere modeling strategy. In

§3 and §4, we present our models of HAT-P-7b and TrES-2. We point out the effects that scattering and nonequilibrium chemistry could have on our models. In §5, we discuss the non-monotonic relationship between the optical opacity in a planet’s upper atmosphere and the planet’s optical emergent radiation. Finally, in §6, we conclude, and in an Appendix, we discuss the various methods used in the literature to represent day-night redistribution in this modeling context.

## 2. ATMOSPHERE MODELING

As in our other recent studies, we use the code COOLTLUSTY (Hubeny et al. 2003; Sudarsky et al. 2003; Burrows et al. 2006, 2008a; Spiegel et al. 2009, 2010), a variant of the code TLUSTY (Hubeny 1988; Hubeny & Lanz 1995), to calculate radiative equilibrium irradiated atmosphere models. Our atomic and molecular opacities are generally calculated assuming chemical equilibrium with solar elemental abundances (Sharp & Burrows 2007; Burrows & Sharp 1999; Burrows et al. 2001, 2002, 2005), although we also calculate a few nonequilibrium models, described in §4. The irradiating spectra in our models are taken from Kurucz (1979, 1994, 2005), interpolated to the effective temperatures and surface gravities of HAT-P-7 and the host star of TrES-2.

In addition to the observationally measured parameters of our models (orbital semimajor axis, planet and stellar radii, planet and stellar surface gravities, stellar effective temperature), and in addition to calculating equilibrium chemistry and radiative transfer, several other physical processes go into our models. These include Rayleigh scattering (Sudarsky et al. 2000; López-Morales & Seager 2007; Burrows et al. 2008b; Rowe et al. 2008), heat redistribution, and the possible presence of an extra optical absorber that could explain the hot upper atmospheres and thermal inversions that have been inferred from infrared observations of several transiting planets. In particular, there are two key free parameters that we vary:  $P_n$  and  $\kappa'$ .

- $P_n$  quantifies the efficiency of day-to-night heat redistribution, and is equal to the fraction of incident day-side heating that is reradiated from the nightside (Burrows et al. 2006, 2008a). In the models in this paper, the redistribution takes place between 0.01 and 0.1 bars.
- $\kappa'$  is an ad hoc extra source of optical absorption opacity in the upper atmosphere, and is motivated by the thermal inversions that have been inferred from the infrared spectra of many exoplanets.  $\kappa'$  is similar to the  $\kappa_e$  of some of our recent work (e.g., Burrows et al. 2008a), except that, rather than a gray optical absorber, it has the same parabolic dependence on frequency as the corresponding

extra absorber in Lopez-Morales et al. (2009) and Burrows et al. (2010).

The models whose properties are plotted in Figs. 1–3 are summarized in Table 1. In addition to these, we also calculate several models with a modification to the code that allows an ad hoc extra source of optical scattering opacity, analogous to  $\kappa'$ , but for scattering instead of absorption.

### 3. HAT-P-7b

HAT-P-7b is a  $1.78M_J$ ,  $1.36R_J$  planet in an approximately circular orbit 0.0377 AU from the  $1.47 M_\odot$ ,  $1.84 R_\odot$ , F6 star HAT-P-7 (Pál et al. 2008). In addition to being in the *Kepler* field, HAT-P-7b is interesting because Rossiter-McLaughlin measurements indicate that it is in a polar or retrograde orbit (Winn et al. 2009; Narita et al. 2009). More relevant to modeling its atmosphere is the fact that, due to its close proximity to a large, relatively hot ( $\sim 6350$  K) star, HAT-P-7b experiences unusually high stellar irradiation ( $\sim 4.8 \times 10^9$  erg cm $^{-2}$  s $^{-1}$  at the substellar point).

As an early confirmation that *Kepler* was performing well, Borucki et al. (2009) published 10 days of commissioning-phase data on HAT-P-7b. These data reveal a surprisingly large secondary eclipse depth in the *Kepler* band ( $\sim 0.43$ – $0.83 \mu\text{m}$ ), as the corresponding planet-star flux ratio decreases by  $(1.3 \pm 0.1) \times 10^{-4}$  when the planet passes behind the star.<sup>2</sup> Borucki et al. (2009) suggest that such a large contrast ratio could imply that the atmosphere absorbs strongly and has minimal redistribution to the night side (low  $P_n$ , in our language). They estimate a day-side temperature of  $2650 \pm 100$  K.

Infrared data for HAT-P-7b became available shortly thereafter, when Christiansen et al. (2010) presented secondary eclipse observations of the planet employing the IRAC instrument on the *Spitzer* Space Telescope. They found planet-star flux-ratios of  $(9.8 \pm 1.7) \times 10^{-4}$ ,  $(15.9 \pm 0.22) \times 10^{-4}$ ,  $(24.5 \pm 3.1) \times 10^{-4}$ , and  $(22.5 \pm 5.2) \times 10^{-4}$  at the IRAC 3.6- $\mu\text{m}$ , 4.5- $\mu\text{m}$ , 5.8- $\mu\text{m}$ , and 8.0- $\mu\text{m}$ , channels, respectively.

Although, as Christiansen et al. (2010) argue, HAT-P-7b’s atmosphere is irradiated strongly enough that it is probably too hot for the condensates that might otherwise be expected to contribute significant scattering opacity, we nevertheless tried adding an ad hoc extra scatterer to the upper atmosphere of some models. We find that the optical point can easily be matched by a model with significant optical scattering, but such models drastically underpredict the *Spitzer* data. Since the Borucki et al. (2009) speculation of an extremely hot

upper atmosphere with low albedo came before the infrared data were published, it might have been a little bit premature. On the other hand, the expectation of low albedo is well motivated by the high stellar irradiation, and seems to be confirmed by the infrared observations.

In Table 1, we present five thermochemical equilibrium models of HAT-P-7b, four having extremely hot upper atmospheres (ranging from H2’s  $\sim 3040$  K to H5’s  $\sim 3180$  K), and a comparison model without a thermal inversion (H1). These five models span a (small) range of values of both  $P_n$  (the degree of day-night redistribution) and  $\kappa'$  (the strength of an ad hoc extra absorber, where the values are in cm $^2$  g $^{-1}$ ). Models with values of  $P_n$  larger than 0.1 are not displayed in this table because such models underpredict the optical data.

The five HAT-P-7b models of Table 1 are displayed in Fig. 1. The top-left and top-right panels portray the wavelength-dependent planet-star flux ratios in the optical and the infrared, respectively, and the corresponding data (Borucki et al. 2009; Christiansen et al. 2010) are superimposed. In both panels, planet and star fluxes are integrated over the relevant bandpasses, and the resulting integrated planet-star ratios are displayed as solid filled circles. The bottom panel shows temperature-pressure profiles for these five models. Models H2-H5, with extra optical opacity, have strong thermal inversions in which the upper atmosphere is heated to temperatures  $\gtrsim 1500$  K greater than they would be in the absence of the extra absorber (as represented by model H1).<sup>3</sup> The near- and mid-infrared spectra for inverted models H2-H5 are nearly indistinguishable from one another, and are all reasonable fits to the IRAC data (although the models are  $\sim 1$ – $2\sigma$  higher than the data at 3.6  $\mu\text{m}$  and 4.5  $\mu\text{m}$ ). Taking into account the optical data (top-left panel), model H5 is the best fit to the available data. HAT-P-7b’s real atmosphere is probably not represented by a 1D radiative equilibrium model, such as model H5, but the available data suggest that significant flux might be absorbed high in the atmosphere, where the radiative timescale is short (Iro et al. 2005; Showman et al. 2008), which would imply that day-side heat would probably be reradiated before much advective redistribution has occurred. The association of high extra opacity with low day-night redistribution in the best-fitting model, therefore, is consistent with what should be expected.

Christiansen et al. (2010) analyzed the thermochemical implications of the *Kepler*/*Spitzer* data, as well. Using the method described in Madhusudhan & Seager (2009) and the four IRAC data points in conjunction with the *Kepler* data, they find

<sup>2</sup> This contrast ratio is similar to the expected dip in flux for an Earth-sized planet passing in front of a Sun-like star, and therefore indicated that *Kepler* should be capable of performing the mission for which it was designed.

<sup>3</sup> The temperature-pressure profiles for models H2-H5 are shown up to extremely low pressures ( $\sim 10^{-8}$  bars), at which point nonequilibrium processes, such as photochemical dissociation and UV opacity, would be important for determining the true thermal profiles.

classes of models that fit the five data points optimally. They find that a blackbody temperature of  $\sim 3175$  K is needed to fit the *Kepler* data, significantly higher than the brightness temperature inferred by Borucki et al. (2009); lower brightness temperatures are inferred for the IRAC data. Their best-fit (non-blackbody) models are (by construction) not in local radiative or chemical equilibrium, but all of the best-fitting models contain thermal inversions, as do our models H2–H5. By relaxing the fit-criterion to  $1.25\text{-}\sigma$  at each datum and allowing strongly nonequilibrium chemical abundances, they find a noninverted model with significant  $\text{CH}_4$  abundance, but the high temperatures of the atmosphere favor CO and therefore favor the inverted models, consistent with our analysis.

#### 4. TRES-2

TrES-2 is a  $1.20M_J$ ,  $1.22R_J$  planet in nearly circular orbit 0.0356 AU from its  $1.06 M_\odot$ ,  $1.00 R_\odot$  solar-type (G0V) star (O’Donovan et al. 2006). At its substellar point, TrES-2 experiences an irradiating flux of  $\sim 1.1 \times 10^9 \text{ erg cm}^{-2} \text{ s}^{-1}$ , similar to that experienced by HD 209458b.

O’Donovan et al. (2010) report IRAC observations of TrES-2, together with nonequilibrium atmosphere models of the planet generated in the manner of Madhusudhan & Seager (2009). O’Donovan et al. find that the infrared data can be reasonably well fit by a blackbody model, a model with a thermal inversion, and a model without a thermal inversion. They point out that their model without a thermal inversion requires a surprisingly low abundance of CO, given the temperature of the atmosphere ( $\sim 1500$  K). Therefore, they favor the model with the inversion.

Here, we consider a variety of models of TrES-2. Motivated by the analysis of O’Donovan et al. (2010), we examine models both with equilibrium and with nonequilibrium chemistry, all of which are in radiative equilibrium. In Table 1, we list five TrES-2 models with opacities defined by equilibrium chemistry at solar abundances (T1–T5) and five that are completely analogous, except with the CO abundance artificially set to 0 (T1n–T5n). In the latter group of models, the carbon that would have been in CO is instead in  $\text{CH}_4$ , and the excess oxygen is instead in  $\text{H}_2\text{O}$ . Among both the set of models with and without CO, there is a model that has no extra absorber and no inversion (T1 and T1n, respectively), and four models that do have an extra absorber and thermal inversions. After we had generated these atmosphere models, Croll et al. (2010) and Kipping & Bakos (2010) published *Ks*-band ( $\sim 2.2 \mu\text{m}$ ) and *Kepler*-band observations, respectively, of TrES-2’s secondary eclipse. The models presented herein can, therefore, be thought of as predictions, not “postdictions,” for the recent data. As a result, it was gratifying to see that the new data are consistent with our predictions, as de-

scribed below.

Figures 2 and 3 portray properties of the atmosphere models with and without CO, respectively. In these figures, similar to Fig. 1, the top-left panel shows the model planet-star flux ratios in the optical and the top-right panel shows the same in the infrared, while the bottom panel shows the temperature-pressure profiles.

We consider first the equilibrium chemistry models in Fig. 2. The non-inverted model (T1) badly fails to reproduce the IRAC data at  $4.5 \mu\text{m}$  and at  $8.0 \mu\text{m}$ . The models with inversions (T2–T5) have similar temperature-pressure profiles to one another. The main difference among these models is the temperature in the region of redistribution ( $10^{-2}$ – $10^{-1}$  bars), where the temperature dip ranges between  $\sim 200$  K (T2;  $P_n = 0.1$ ) and  $\sim 700$  K (T4, T5;  $P_n = 0.3$ ). As a consequence of their similarity, these four profiles correspond to very similar flux ratios at  $4.5 \mu\text{m}$ ,  $5.8 \mu\text{m}$ , and  $8.0 \mu\text{m}$ . Model T5 ( $\kappa' = 0.3 \text{ cm}^2 \text{ g}^{-1}$ ) is the best fit at  $3.6 \mu\text{m}$ , but the inverted models all overpredict the  $5.8 \mu\text{m}$ -point by  $\sim 2\sigma$ . Models T2–T5 all predict *Ks*-band flux consistent with the Croll et al. (2010) observations. All five models predict very low planet-star flux ratios in the optical, in contrast to the models and the *Kepler* observation of HAT-P-7b (for which  $F_p/F_* = 1.3 \times 10^{-4}$ ; see §3). Aside from model T1, which is clearly disfavored by the IRAC data, the other models all predict planet-star flux ratios of  $\lesssim 2 \times 10^{-5}$ . With no extra absorber, model T1 still predicts a *Kepler*-band flux ratio of only  $\sim 3 \times 10^{-5}$ . Models T2–T5 are all consistent with the Kipping & Bakos (2010) observation of  $(1.1 \pm 0.7) \times 10^{-5}$  ( $2\text{-}\sigma$  errors).

The models without CO opacity (T1n–T5n), portrayed in Fig. 3, are qualitatively quite similar to the equilibrium models in all our diagnostics (optical flux, infrared flux, and thermal profile). However, there are some differences in detail. The deep isothermal layers of all five models are hotter by  $\sim 150$  K than their equilibrium counterparts, and the upper atmosphere of the inverted models (T2n–T5n) is cooler by a comparable amount, while the upper atmosphere of the non-inverted model (T1n) is still warmer than its equilibrium analog (T1). The magnitude of the temperature dip in the redistribution range is also somewhat muted compared with the equilibrium models. These slight  $T$ - $P$  profile differences, in conjunction with the altered opacities, result in slightly different optical and infrared spectra. In the infrared, the inverted no-CO models produce lower flux at  $5.8 \mu\text{m}$ , overpredicting the observed data by less than the equilibrium models. Among no-CO models, the IRAC data are best fit by a model with slightly less extra optical absorption (T4n,  $\kappa' = 0.2 \text{ cm}^2 \text{ g}^{-1}$ ). These models have optical fluxes that are qualitatively similar to their equilibrium counterparts, all predicting *Kepler* band flux ratios of  $\lesssim 5 \times 10^{-5}$ . In particular,

model T1n predicts slightly higher optical flux than does model T1, but the inverted models T2n–T5n predict slightly lower optical fluxes than do models T2–T5. The predicted *Ks*-band and *Kepler*-band fluxes of models T3n–T5n are all consistent with observations of Croll et al. (2010) and Kipping & Bakos (2010), respectively.

The basic conclusion that we draw from examining models with reduced CO opacity is that even such a drastic reduction of CO abundance as entirely eliminating it does not cause dramatic changes in thermal profiles or spectra. In the analysis of O’Donovan et al. (2010), changing the  $[\text{CO}]:[\text{CH}_4]:[\text{CO}_2]$  ratio from  $10^{-6} : 10^{-6} : 0$  (i.e., 1:1:0) to  $10^{-4} : 5 \times 10^{-5} : 2 \times 10^{-6}$  (i.e., 50:25:1), together with changing the temperature-pressure profile from a non-inverted to an inverted one, results in a modest improvement in the quality of the fit (particularly at  $8\text{-}\mu\text{m}$ ). We note that, in addition to having a surprisingly nonequilibrium  $[\text{CO}]:[\text{CH}_4]$  ratio, the O’Donovan et al. (2010) noninverted model has a very low total abundance of carbon. Even though their inverted model is substantially subsolar in carbon (by more than an order of magnitude), reducing the carbon abundance by another two orders of magnitude is nearly tantamount to removing carbon from the opacities entirely. In sum, our analysis shows that, among models with solar abundance of carbon, the presence or absence of CO in the database does not make a large difference in the thermal profiles or in the emergent spectra, and in either case way a hot upper atmosphere and thermal inversion are required in the model in order to come at all close to matching the IRAC data. Individual molecular abundances substantially different from what one would obtain for solar elemental abundances might allow for marginally improved fits to the data, but might not yet be called for by the relatively sparse data available so far.

The upper left panels of both Figs. 2 and 3 both show that models with extra optical absorbers in the upper atmosphere have *lower* planet-star flux ratios in the *Kepler* band than the models without an extra absorber. We revisit this point in §5. In light of this generic trend, and since among radiative equilibrium models the IRAC data are better fit by inverted models than by non-inverted models, we predict that *Kepler* photometry of TrES-2 will indicate low optical flux from this planet, not more than one or a few times  $10^{-5}$  of the stellar flux. If future *Kepler*-band observations reveal optical flux in excess of this amount, that might be indicative of extra optical scattering opacity that was not included in our models.

## 5. OPTICAL FLUX VS. OPTICAL ABSORBER STRENGTH

Here, we point out a puzzle: the upper left panel of Fig. 1 shows a different trend of optical flux vs.  $\kappa'$  from the analogous panels of Figs. 2 and 3. López-

Morales & Seager (2007) noted that inverted models, with their hot upper atmospheres, might be expected to have higher optical flux than non-inverted models. But how do we explain the trend seen for TrES-2 (Figs. 2 and 3)?

If there is an extra absorber in the optical part of the spectrum (a  $\kappa_e$ , in the terminology of Burrows et al. 2008b, or a  $\kappa'$  in the present work), the emergent optical flux is affected by two competing effects. The absorber makes the planet darker at altitude, but can also heat the upper atmosphere. The latter effect makes the upper atmosphere of the planet more emissive.

Figure 4 illustrates how the balance of these two effects depends on the opacity ( $\kappa'$ ) of the upper-atmosphere absorber, in both HAT-P-7b and TrES-2. The *Kepler* bandpass brightness of  $P_n = 0.0$  models of both planets (HAT-P-7b: green; TrES-2: blue) is plotted as a function of  $\kappa'$ , for a series of values of  $\kappa'$  between 0 and  $1.1 \text{ cm}^2 \text{ g}^{-1}$ . For both planets, a small amount of extra absorption results in reduced emergent flux in the *Kepler* band, and, for both planets, large values of  $\kappa'$  ( $\gtrsim 0.3 \text{ cm}^2 \text{ g}^{-1}$ ) result in increased optical emission, as emission from the Wien tail of the hot upper atmosphere becomes more prominent in the optical part of the spectrum. There is, therefore, a generic non-monotonic character to the dependence of optical flux on  $\kappa'$ . The degree of the non-monotonicity, however, is greater for HAT-P-7b models than for TrES-2 models. In the former, the optical flux for  $\kappa' \gtrsim 0.3 \text{ cm}^2 \text{ g}^{-1}$  is greater than with no extra absorption, while in the latter, even with  $\kappa' = 1.1 \text{ cm}^2 \text{ g}^{-1}$  the optical flux is just over half of what it is with no extra absorption. The origin of this difference is related to the properties of the irradiation. HAT-P-7 is an exceptionally large ( $1.84 R_\odot$ ) star that is fairly hot (F6, 6350 K), whereas TrES-2’s star is a more ordinary solar-type star ( $1.003 R_\odot$ , G0V, 5850 K). As a result, the incident optical irradiation at HAT-P-7b is more than 4 times as great as on TrES-2. This greatly enhanced incident optical irradiation results in a much greater sensitivity to the presence of an extra optical absorber.

## 6. CONCLUSION

We have presented atmosphere models of HAT-P-7b and TrES-2, two of the three *Kepler* field planets that were known prior to the start of the *Kepler* mission. We find that the combination of the IRAC and *Kepler* secondary eclipse data for HAT-P-7b, with a *Kepler*-bandpass secondary eclipse ratio of  $\sim 1.3 \times 10^{-4}$ , appear to require an extremely hot upper atmosphere, with an extra optical absorber that creates a strong thermal inversion and with little day-night redistribution. The IRAC data for TrES-2 led us to expect that TrES-2 has a much lower planet-star flux ratio ( $\lesssim 2 \times 10^{-5}$ ) in the *Kepler* bandpass than does the HAT-P-7 system, and indeed this is what was seen in recently published

*Kepler* data of this object.

Furthermore, we find that there is a non-monotonic relationship between  $\kappa'$  and a planet's day-side emergent optical flux. This non-monotonicity highlights the need for multiwavelength observations in order to better estimate the atmospheric structure.

grant NNX07AG80G. We also acknowledge support through JPL/Spitzer Agreements 1328092, 1348668, and 1312647. The authors are pleased to acknowledge that part of this research was performed while in residence at the Kavli Institute for Theoretical Physics, and was supported in part by the National Science Foundation under Grant No. PHY05-51164.

We thank Ivan Hubeny, Laurent Ibgui, Kevin Heng, and Jason Nordhaus for useful discussions. We also appreciate the careful reading and helpful comments from the referee, Giovanna Tinetti. This study was supported in part by NASA

## APPENDIX

### PARAMETERIZING REDISTRIBUTION IN A 1D MODEL

There have been several approaches used in the literature for treating the redistribution of day-side irradiation to the nightside in the context of one-dimensional models. Here, we consider several parameterizations and the relationships among them. Early work, including that of our group prior to Burrows et al. (2006), used only a single parameter (called “ $f$ ”) to describe redistribution. However, there are at least three effects that ought to be included in a description of how an atmosphere redistributes heat: (1) some fraction of incident energy is transported to the nightside via atmospheric motions (we call this fraction “ $P_n$ ”); (2) this redistribution occurs at some depth between the top and the bottom of the atmosphere; and (3) the visible face of the planet (the dayside at secondary eclipse phase) has (in general) an anisotropic distribution of specific intensity in the direction of Earth. Our more recent work, including this paper, employs our attempt, however imperfect, to incorporate these physical effects that 1D models from other groups have not fully included. In particular, when other modeling efforts have implemented schemes for day-night heat transport, they have essentially taken the redistribution to occur before the incoming radiation reaches the top of the atmosphere. In contrast, we specify the range of pressures at which the redistribution occurs; while our numerical choice might be not be accurate in detail, it is a physically motivated, less ad hoc way to parameterize the physics that we know affect emergent spectra.

One of the best-known redistribution parameters is the aforementioned geometrical  $f$  factor, which arises from an energy balance relation of the following form:

$$L_p = \frac{\pi}{f} R_p^2 \sigma T_{\text{unif}}^4, \quad (1)$$

$$\text{or, } \frac{F_p}{F_*} = f \left( \frac{R_p}{a} \right)^2. \quad (2)$$

In eq. (1),  $L_p \equiv (\pi R_p^2) L_* / (4\pi a^2)$  is the total stellar power intercepted by the planet (and, therefore, approximately equals the emergent radiation from the planet),  $R_p$  is the planet's radius,  $L_*$  is the stellar luminosity,  $a$  is the orbital separation,  $\sigma$  is the Stefan-Boltzmann constant, and  $T_{\text{unif}}$  is the temperature of a uniform-temperature sphere of radius  $R_p$  whose flux at Earth near secondary eclipse phase would be the same as that of the planet. In eq. (2),  $F_p$  is the integrated flux from the planet at Earth,<sup>4</sup> and  $F_*$  is the integrated stellar flux. In eqs. (1) and (2), and in the remainder of this section, we have ignored both scattering in the planet's atmosphere and its own intrinsic luminosity (from its heat of formation, tidal heating, etc.). The  $f$  factor has been used by a number of authors in the last decade (Burrows et al. 2003, 2005; Fortney et al. 2005; López-Morales & Seager 2007; Hansen 2008; and referred to as  $\alpha$  in Barman et al. 2005).<sup>5</sup> Perfect redistribution (implying that the planet is itself of uniform temperature) corresponds to  $f = 1/4$ . Zero

<sup>4</sup>  $F_p = \sigma T_{\text{unif}}^4 (R_p/d)^2$ , where  $d$  is the distance from the planet to Earth.

<sup>5</sup> We note that Burrows et al. (2008a) also use a parameter called  $f$ , but this  $f$  (which is typically set to 2/3) represents the direction-cosine of incident irradiation that is used in the planar atmosphere calculation, and is therefore related to distribution of temperature on the dayside, instead of to the fraction of energy that is redistributed to the nightside. Some work (e.g. that of Barman et al. 2005) integrates the contributions to the total planet-flux at Earth of a series of concentric annuli, from the substellar point to the terminator. Burrows et al. (2008a) show that this integral is extremely well-approximated by taking the entire visible hemisphere as being irradiated by the ray at direction-cosine 2/3.

redistribution, so that each annulus a given angle away from the substellar point absorbs and reradiates its local irradiation isotropically, corresponds to  $f = 2/3$ .<sup>6</sup> There is, thus, a “beaming factor” that increases  $f$  by a factor of 4/3 over the value (1/2) that it would have if the dayside were of uniform temperature instead of peaked toward the center of the disk in accordance with the irradiating flux.  $f$  is typically implemented in 1D atmosphere models as simply a uniform reduction of the incident flux at the top of the atmosphere (algorithmically, though not physically, equivalent to the effect of albedo).

Alternatively, we may characterize the redistribution by removing a fraction  $P_n$  of the incident stellar flux on the dayside in a prescribed pressure interval (as described in §2), and inserting the energy at a similar (or different) level on the nightside. In such a prescription,  $P_n$  plausibly ranges between 0 (corresponding to no redistribution) and 0.5 (corresponding to the nightside radiating as much power as the dayside, via redistributive winds). Burrows et al. (2006), Burrows et al. (2008a), and other work from our group implement this procedure. In order to calculate theoretical secondary eclipse fluxes and spectra, one must have a model of the three-dimensional distribution of temperature in a planet’s atmosphere (e.g., Showman et al. 2008, 2009; Burrows et al. 2010). In lieu of performing three-dimensional dynamical calculations, our 1D atmosphere models assume the same beaming factor for day-side emergent radiation, regardless of the total day-side radiance; and they assume uniform temperature on the nightside. In particular, on the dayside, when  $P_n = 0.5$ ,  $f = 1/3$  (which is 4/3 of the 1/4 that  $f$  would equal for a uniform-temperature dayside, when half the incident flux has been redistributed to the nightside). More generally, the integrated model day-side flux from the planet can be approximately described by eq. (2), taking  $f$  to be defined by

$$f = \frac{2}{3}(1 - P_n). \quad (3)$$

The descriptions in Cowan et al. (2007) of how “ $T_{\text{day}}$ ” and “ $T_{\text{night}}$ ” depend on  $P_n$  correctly quantify the total emission from the day and night sides of the planet, but they do not include the beaming caused by an anisotropic temperature distribution on the dayside that is peaked at the substellar point; therefore, unlike what is suggested in Cowan et al. (2007), the integrated day-side flux is not described by taking the dayside to be of uniform temperature  $T_{\text{day}}$ .

Yet a third redistribution parameter,  $\varepsilon$ , is suggested by Cowan & Agol (2010).  $\varepsilon$  ranges between 0 (no redistribution) and 1 (full redistribution). It initially appears to be defined similarly to  $P_n$ , and is described (in part) by the following relation:

$$L_p = \frac{\pi}{(8 - 5\varepsilon)/12} R_p^2 \sigma \tilde{T}_{\text{day}}^4, \quad (4)$$

where  $\tilde{T}_{\text{day}}$  is the same as  $T_{\text{unif}}$  of eq. (1), i.e., a measure of the flux in the direction of Earth. In eq. (4), there is a tilde above the expression for day-side temperature to distinguish it from the corresponding expression in Cowan et al. (2007), which is a measure of the total day-side emission, as opposed to the flux in the direction of Earth. Comparing eqs. (1) and (4) shows that  $\varepsilon$  is a rescaling of  $f$ :  $\varepsilon = (8 - 12f)/5$ . Cowan & Agol suggest that their  $\varepsilon = 0$  limit produces a brighter dayside than does the  $P_n = 0$  limit, but it does not. Instead, the  $P_n = 0.5$  limit produces a brighter dayside than does the  $\varepsilon = 1$  limit (brighter by the beaming factor of 4/3).

Finally, we emphasize that while eqs. (2) and (3) describe how the integrated planet flux depends on  $P_n$ , this parameter does more than simply affect the top-of-atmosphere energy budget. The real benefit of  $P_n$  (which is not captured by the above equations) is that, when nonzero, instead of reducing incident irradiation, it removes energy from the dayside (and deposits it on the nightside) at more realistic levels in the atmosphere. This process contributes to a slight thermal inversion by cooling the middle atmosphere, and, therefore, affects the ratio of 3.6- $\mu\text{m}$  flux to the 4.5- $\mu\text{m}$  flux in a way that is not reproduced by the standard  $f$  parameterizations in which incident irradiation is reduced at the top of the atmosphere.

<sup>6</sup> In this case, the specific intensity in the direction of Earth from a annulus at direction-cosine  $\mu$  away from the substellar point (at full-moon phase) is proportional to  $\mu$ . Specifically,  $I[\mu] = \mu L_*/(2\pi a)^2$ .

## REFERENCES

- Barman, T. S., Hauschildt, P. H., & Allard, F. 2005, *ApJ*, 632, 1132
- Borucki, W. J., Koch, D., Jenkins, J., Sasselov, D., Gilliland, R., Batalha, N., Latham, D. W., Caldwell, D., Basri, G., Brown, T., Christensen-Dalsgaard, J., Cochran, W. D., DeVore, E., Dunham, E., Dupree, A. K., Gautier, T., Geary, J., Gould, A., Howell, S., Kjeldsen, H., Lissauer, J., Marcy, G., Meibom, S., Morrison, D., & Tarter, J. 2009, *Science*, 325, 709
- Burrows, A., Budaj, J., & Hubeny, I. 2008a, *ApJ*, 678, 1436
- Burrows, A., Dulick, M., Bauschlicher, Jr., C. W., Bernath, P. F., Ram, R. S., Sharp, C. M., & Milsom, J. A. 2005, *ApJ*, 624, 988
- Burrows, A., Hubbard, W. B., Lunine, J. I., & Liebert, J. 2001, *Reviews of Modern Physics*, 73, 719
- Burrows, A., Hubeny, I., Budaj, J., Knutson, H. A., & Charbonneau, D. 2007, *ApJ*, 668, L171
- Burrows, A., Ibgui, L., & Hubeny, I. 2008b, *ApJ*, 682, 1277
- Burrows, A., Ram, R. S., Bernath, P., Sharp, C. M., & Milsom, J. A. 2002, *ApJ*, 577, 986
- Burrows, A., Rauscher, E., Spiegel, D., & Menou, K. 2010, *ArXiv e-prints*
- Burrows, A. & Sharp, C. M. 1999, *ApJ*, 512, 843
- Burrows, A., Sudarsky, D., & Hubbard, W. B. 2003, *ApJ*, 594, 545
- Burrows, A., Sudarsky, D., & Hubeny, I. 2006, *ApJ*, 650, 1140
- Christiansen, J. L., Ballard, S., Charbonneau, D., Madhusudhan, N., Seager, S., Holman, M. J., Wellnitz, D. D., Deming, D., A'Hearn, M. F., & the EPOXI Team. 2010, *ApJ*, 710, 97
- Cowan, N. B. & Agol, E. 2010, *ArXiv e-prints*
- Cowan, N. B., Agol, E., & Charbonneau, D. 2007, *MNRAS*, 379, 641
- Croll, B., Albert, L., Lafrenière, D., Jayawardhana, R., & Fortney, J. J. 2010, *ArXiv e-prints*
- Fortney, J. J., Cooper, C. S., Showman, A. P., Marley, M. S., & Freedman, R. S. 2006, *ApJ*, 652, 746
- Fortney, J. J., Lodders, K., Marley, M. S., & Freedman, R. S. 2008, *ApJ*, 678, 1419
- Fortney, J. J., Marley, M. S., Hubickyj, O., Bodenheimer, P., & Lissauer, J. J. 2005, *Astronomische Nachrichten*, 326, 925
- Hansen, B. M. S. 2008, *ApJS*, 179, 484
- Holman, M. J., Winn, J. N., Latham, D. W., O'Donovan, F. T., Charbonneau, D., Torres, G., Sozzetti, A., Fernandez, J., & Everett, M. E. 2007, *ApJ*, 664, 1185
- Hubeny, I. 1988, *Computer Physics Communications*, 52, 103
- Hubeny, I., Burrows, A., & Sudarsky, D. 2003, *ApJ*, 594, 1011
- Hubeny, I. & Lanz, T. 1995, *ApJ*, 439, 875
- Iro, N., Bézard, B., & Guillot, T. 2005, *A&A*, 436, 719
- Kipping, D. M. & Bakos, G. Á. 2010, *ArXiv e-prints*
- Knutson, H. A., Charbonneau, D., Allen, L. E., Burrows, A., & Megeath, S. T. 2008, *ApJ*, 673, 526
- Knutson, H. A., Howard, A. W., & Isaacson, H. 2010, *ArXiv e-prints*
- Kurucz, R. 1994, *Solar abundance model atmospheres for 0.1,2,4,8 km/s. Kurucz CD-ROM No. 19. Cambridge, Mass.: Smithsonian Astrophysical Observatory*, 1994., 19
- Kurucz, R. L. 1979, *ApJS*, 40, 1
- . 2005, *Memorie della Societa Astronomica Italiana Supplement*, 8, 14
- Li, J. & Goodman, J. 2010, *ArXiv e-prints*
- López-Morales, M., Coughlin, J. L., Sing, D. K., Burrows, A., Apai, D., Rogers, J. C., & Spiegel, D. S. 2009, *ArXiv e-prints*
- López-Morales, M. & Seager, S. 2007, *ApJ*, 667, L191
- Madhusudhan, N. & Seager, S. 2009, *ApJ*, 707, 24
- . 2010, *ArXiv e-prints*
- Mislis, D. & Schmitt, J. H. M. M. 2009, *A&A*, 500, L45
- Narita, N., Sato, B., Hirano, T., & Tamura, M. 2009, *ArXiv e-prints*
- O'Donovan, F. T., Charbonneau, D., Harrington, J., Madhusudhan, N., Seager, S., Deming, D., & Knutson, H. A. 2010, *ApJ*, 710, 1551
- O'Donovan, F. T., Charbonneau, D., Mandushev, G., Dunham, E. W., Latham, D. W., Torres, G., Sozzetti, A., Brown, T. M., Trauger, J. T., Belmonte, J. A., Rabus, M., Almenara, J. M., Alonso, R., Deeg, H. J., Esquerdo, G. A., Falco, E. E., Hillenbrand, L. A., Roussanova, A., Stefanik, R. P., & Winn, J. N. 2006, *ApJ*, 651, L61
- Pál, A., Bakos, G. Á., Torres, G., Noyes, R. W., Latham, D. W., Kovács, G., Marcy, G. W., Fischer, D. A., Butler, R. P., Sasselov, D. D., Sipőcz, B., Esquerdo, G. A., Kovács, G., Stefanik, R., Lázár, J., Papp, I., & Sári, P. 2008, *ApJ*, 680, 1450
- Rabus, M., Deeg, H. J., Alonso, R., Belmonte, J. A., & Almenara, J. M. 2009, *ArXiv e-prints*
- Raetz, S., Mugrauer, M., Schmidt, T. O. B., Roell, T., Eisenbeiss, T., Hohle, M., Seifahrt, A., Koeltzsch, A., Vaňko, M., Broeg, C., Koppenhoefer, J., & Neuhäuser, R. 2009, in *IAU Symposium*, Vol. 253, *IAU Symposium*, 436–439
- Richardson, L. J., Deming, D., Horning, K., Seager, S., & Harrington, J. 2007, *Nature*, 445, 892
- Rowe, J. F., Matthews, J. M., Seager, S., Miller-Ricci, E., Sasselov, D., Kuschnig, R., Guenther, D. B., Moffat, A. F. J., Rucinski, S. M., Walker, G. A. H., & Weiss, W. W. 2008, *ApJ*, 689, 1345
- Sharp, C. M. & Burrows, A. 2007, *ApJS*, 168, 140
- Showman, A. P., Cooper, C. S., Fortney, J. J., & Marley, M. S. 2008, *ApJ*, 682, 559
- Showman, A. P., Fortney, J. J., Lian, Y., Marley, M. S., Freedman, R. S., Knutson, H. A., & Charbonneau, D. 2009, *ApJ*, 699, 564
- Sozzetti, A., Torres, G., Charbonneau, D., Latham, D. W., Holman, M. J., Winn, J. N., Laird, J. B., & O'Donovan, F. T. 2007, *ApJ*, 664, 1190
- Spiegel, D. S., Burrows, A., Ibgui, L., Hubeny, I., & Milsom, J. A. 2010, *ApJ*, 709, 149
- Spiegel, D. S., Silverio, K., & Burrows, A. 2009, *ApJ*, 699, 1487
- Sudarsky, D., Burrows, A., & Hubeny, I. 2003, *ApJ*, 588, 1121
- Sudarsky, D., Burrows, A., & Pinto, P. 2000, *ApJ*, 538, 885
- Tinetti, G., Liang, M., Vidal-Madjar, A., Ehrenreich, D., Lecavelier des Etangs, A., & Yung, Y. L. 2007, *ApJ*, 654, L99
- Tinetti, G., Meadows, V. S., Crisp, D., Fong, W., Velusamy, T., & Snively, H. 2005, *Astrobiology*, 5, 461
- Welsh, W. F., Orosz, J. A., Seager, S., Fortney, J. J., Jenkins, J., Rowe, J. F., Koch, D., & Borucki, W. J. 2010, *ApJ*, 713, L145
- Winn, J. N., Johnson, J. A., Albrecht, S., Howard, A. W., Marcy, G. W., Crossfield, I. J., & Holman, M. J. 2009, *ApJ*, 703, L99
- Youdin, A. N. & Mitchell, J. L. 2010, *ArXiv e-prints*
- Zahnle, K., Marley, M. S., Freedman, R. S., Lodders, K., & Fortney, J. J. 2009, *ApJ*, 701, L20



TABLE 1  
HAT-P-7B AND TRÉS-2 MODELS

Model	$P_n$	$\kappa'$ ( $\text{cm}^2 \text{ g}^{-1}$ )	Chemistry
H1 <sup>a</sup>	0.10	0.0	equilibrium
H2	0.05	0.4	equilibrium
H3	0.10	0.7	equilibrium
H4	0.10	1.1	equilibrium
H5	0.00	1.1	equilibrium
T1 <sup>b</sup>	0.2	0.0	equilibrium
T2	0.1	0.2	equilibrium
T3	0.2	0.2	equilibrium
T4	0.3	0.2	equilibrium
T5	0.3	0.3	equilibrium
T1n	0.2	0.0	no CO <sup>c</sup>
T2n	0.1	0.2	no CO
T3n	0.2	0.2	no CO
T4n	0.3	0.2	no CO
T5n	0.3	0.3	no CO

<sup>a</sup>Models H1–H5 have the following parameters – orbital semimajor axis ( $a$ ), planet and stellar surface gravity ( $g_p$ ,  $g_*$ ), planet and stellar radii ( $R_p$ ,  $R_*$ ), and stellar effective temperature  $T_*$  – appropriate to the HAT-P-7 system ( $a = 0.0377$  AU;  $\log_{10} g_p = 3.38$ ,  $\log_{10} g_* = 4.08$  where  $g_p$ ,  $g_*$  are in cgs;  $R_p = 1.363R_J$ , where  $R_J \equiv 7.15 \times 10^9$  cm is Jupiter’s radius;  $R_* = 1.84R_\odot$ ;  $T_* = 6350$  K). The irradiating spectrum is interpolated from Kurucz models.

<sup>b</sup>Models T1–T5 and T1n–T5n have parameters appropriate to the TrÉS-2 system ( $a = 0.0356$  AU;  $\log_{10} g_p = 3.30$ ,  $\log_{10} g_* = 4.43$  where  $g_p$ ,  $g_*$  are in cgs;  $R_p = 1.224R_J$ ;  $R_* = 1.003R_\odot$ ;  $T_* = 5850$  K).

<sup>c</sup>Models T1n–T5n have opacities defined by out-of-equilibrium chemistry, where CO has been artificially removed, with the carbon instead in  $\text{CH}_4$  and the excess oxygen instead in  $\text{H}_2\text{O}$ .

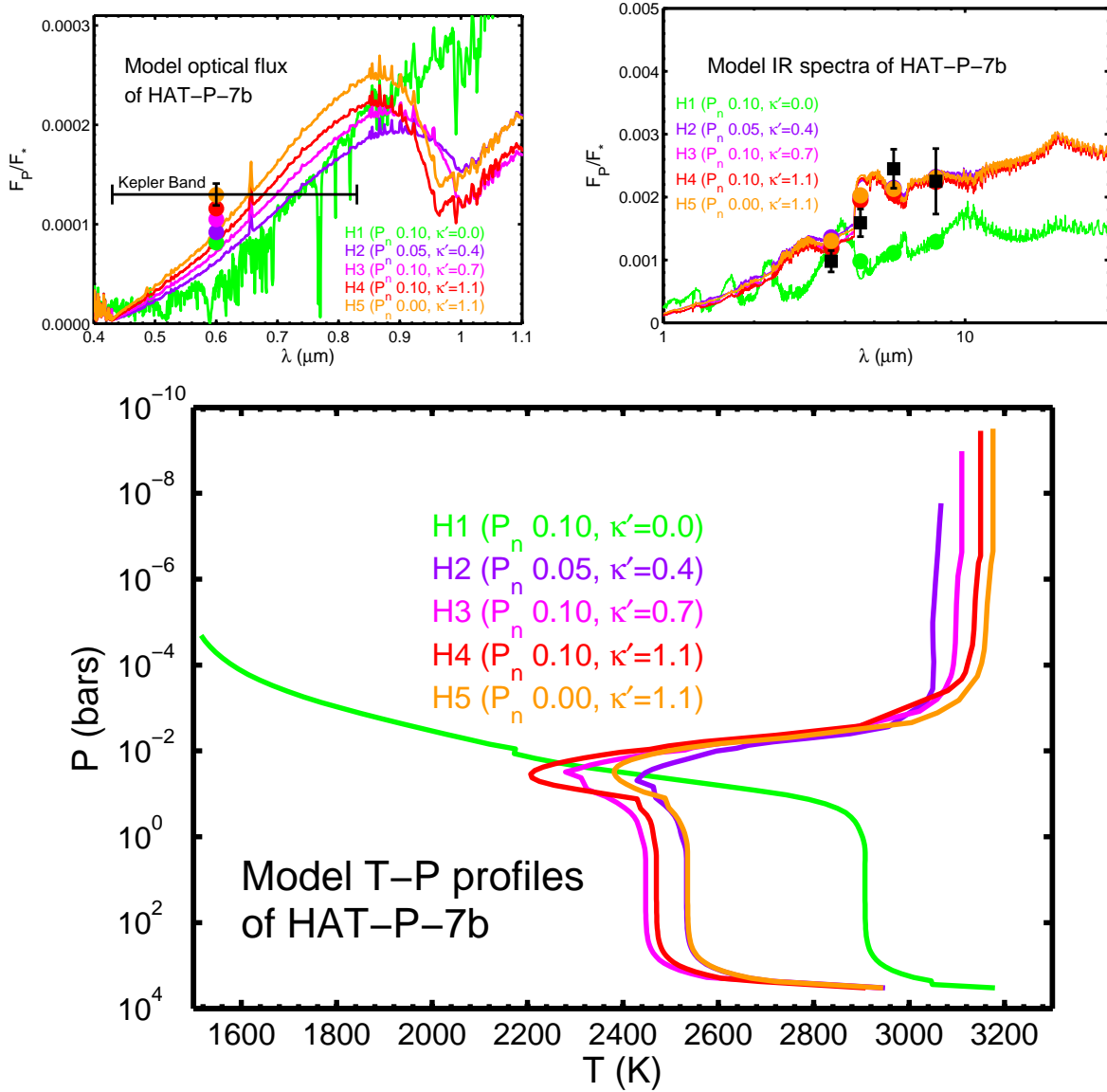


FIG. 1.— HAT-P-7b model atmospheres. The models (H1–H5) encompass varying degrees of redistribution (parameterized as  $P_n$ ) and upper-atmosphere optical absorption (parameterized as  $\kappa'$ , where the values are in  $\text{cm}^2 \text{g}^{-1}$ ), and are listed in Table 1. Measured data are shown where available. *Top left:* Optical planet-star flux ratios. The data point (indicated by the  $1\text{-}\sigma$  error bars) is from Borucki et al. (2009), and the horizontal black line indicates the full width at 10% maximum of the *Kepler* bandpass. The filled colored circles show the integrals of the model flux over the *Kepler* bandpass. The model that fits the data best is H5, which has significant upper-atmosphere absorption ( $\kappa' = 1.1 \text{ cm}^2 \text{g}^{-1}$ ) and no redistribution. *Top Right:* Infrared planet-star flux ratios. The data points with  $1\text{-}\sigma$  error bars are IRAC data from Christiansen et al. (2010). Filled colored circles show the integrals of models over the response functions for the IRAC bands. Among models with significant upper-atmosphere absorption (models H2–H5), there is little difference in the infrared spectrum. Model H5 is a slightly better fit than H2, a slightly worse fit than H3 and H4 at  $3.6 \mu\text{m}$ , and is a slightly worse fit than models H2–H4 at  $4.5 \mu\text{m}$ . The models fit the  $5.8\text{-}\mu\text{m}$  and  $8.0\text{-}\mu\text{m}$  IRAC data equally well. *Bottom:* Temperature-pressure profiles. The models with extra optical absorption in the upper atmosphere (models H2–H5) all show large thermal inversions, with upper-atmosphere temperatures  $\sim 1500 \text{ K}$  or more hotter than what would be expected in the absence of extra heating (indicated by model H1). Note that our models with an extra absorber extend to very low pressures ( $\sim 10^{-8}$  bars), where other physics in the thermosphere might be important in determining the actual radiative equilibrium thermal profile.

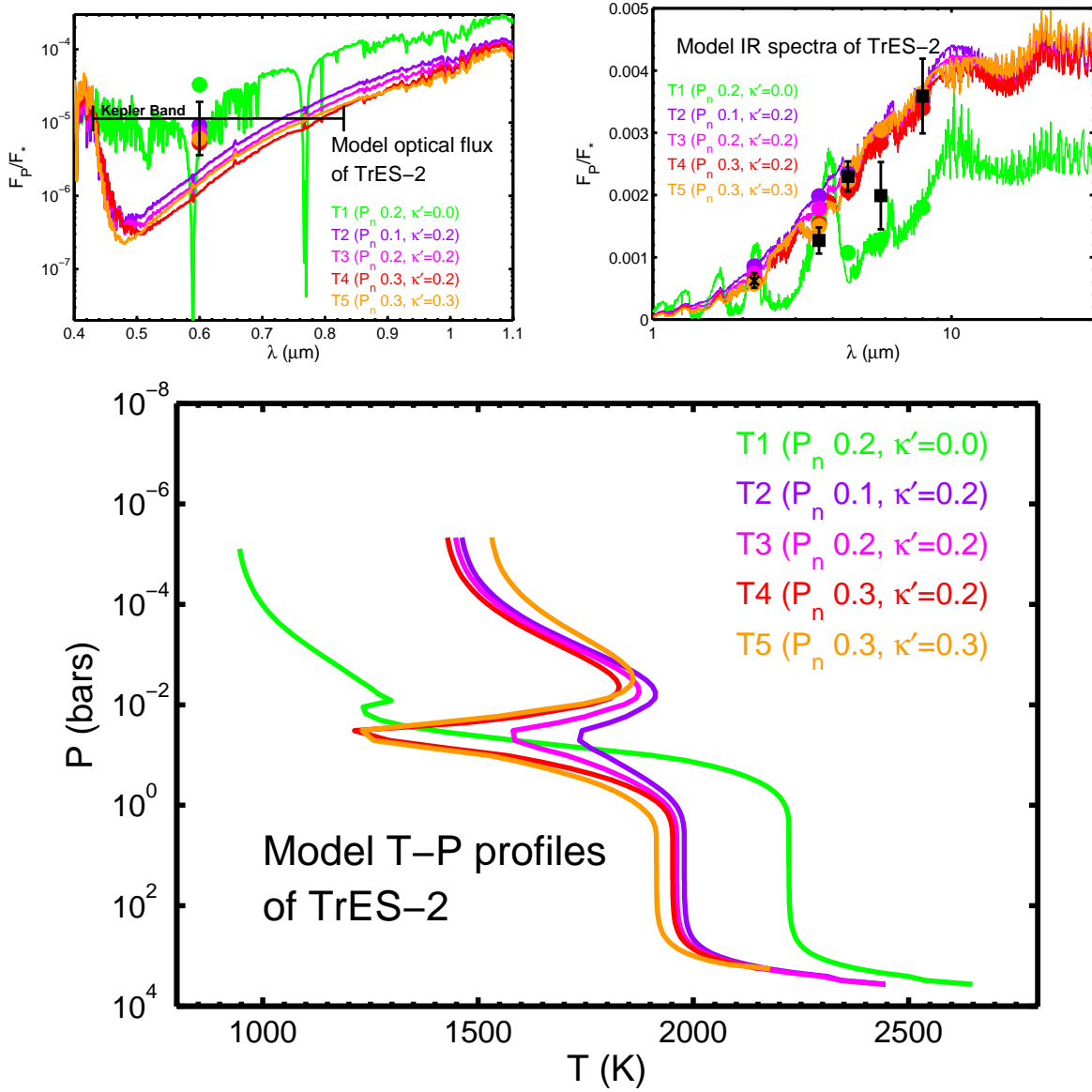


FIG. 2.— TrES-2 equilibrium chemistry model atmospheres, analogous to Fig. 1, but for TrES-2 instead of HAT-P-7b. The models (T1–T5) encompass varying degrees of heat redistribution ( $P_n$ ) and upper-atmosphere optical absorption ( $\kappa'$ , values in  $\text{cm}^2 \text{g}^{-1}$ ), and are listed in Table 1. *Top left:* Optical planet-star flux ratios (log scale). The horizontal black line indicates the full width at 10% maximum of the *Kepler* bandpass, and is at the level of the data (shown with with  $2\text{-}\sigma$  vertical error bars) from Kipping & Bakos (2010). The filled colored circles show the integrals of the model flux over the *Kepler* bandpass. Models with upper atmosphere absorption (T2–T5) tend to have low optical flux ( $F_p/F_* \lesssim 2 \times 10^{-5}$ ). Even with  $\kappa' = 0 \text{ cm}^2 \text{g}^{-1}$  (model T1), the optical flux ratio is  $\sim 3 \times 10^{-5}$ . Models T2–T5 are all consistent with the data, to  $2\sigma$ . *Top Right:* Infrared planet-star flux ratios. The black square data points with  $1\text{-}\sigma$  error bars are IRAC data from O’Donovan et al. (2010), and the black cross data point (with  $1\text{-}\sigma$  error bars) represents *Ks*-band data from Croll et al. (2010). Filled colored circles show the integrals of models over the response functions for the IRAC bands (at 3.6, 4.5, 5.8, and 8.0  $\mu\text{m}$ ) and for *Ks*-band (at 2.2  $\mu\text{m}$ ). The 4.5- $\mu\text{m}$ , 5.8- $\mu\text{m}$ , and 8.0- $\mu\text{m}$  IRAC data clearly favor models with some extra absorption. At 3.6  $\mu\text{m}$ , 4.5  $\mu\text{m}$ , and 8.0  $\mu\text{m}$ , model T5 is a good fit to the data, but it misses the data by  $\sim 2\sigma$  at 5.8  $\mu\text{m}$ . *Bottom:* Temperature-pressure profiles. The models with extra optical absorption in the upper atmosphere (models T2–T5) show moderate thermal inversions, with upper-atmosphere temperatures  $\sim 500$  K hotter than what would be expected in the absence of extra heating (indicated by model T1).

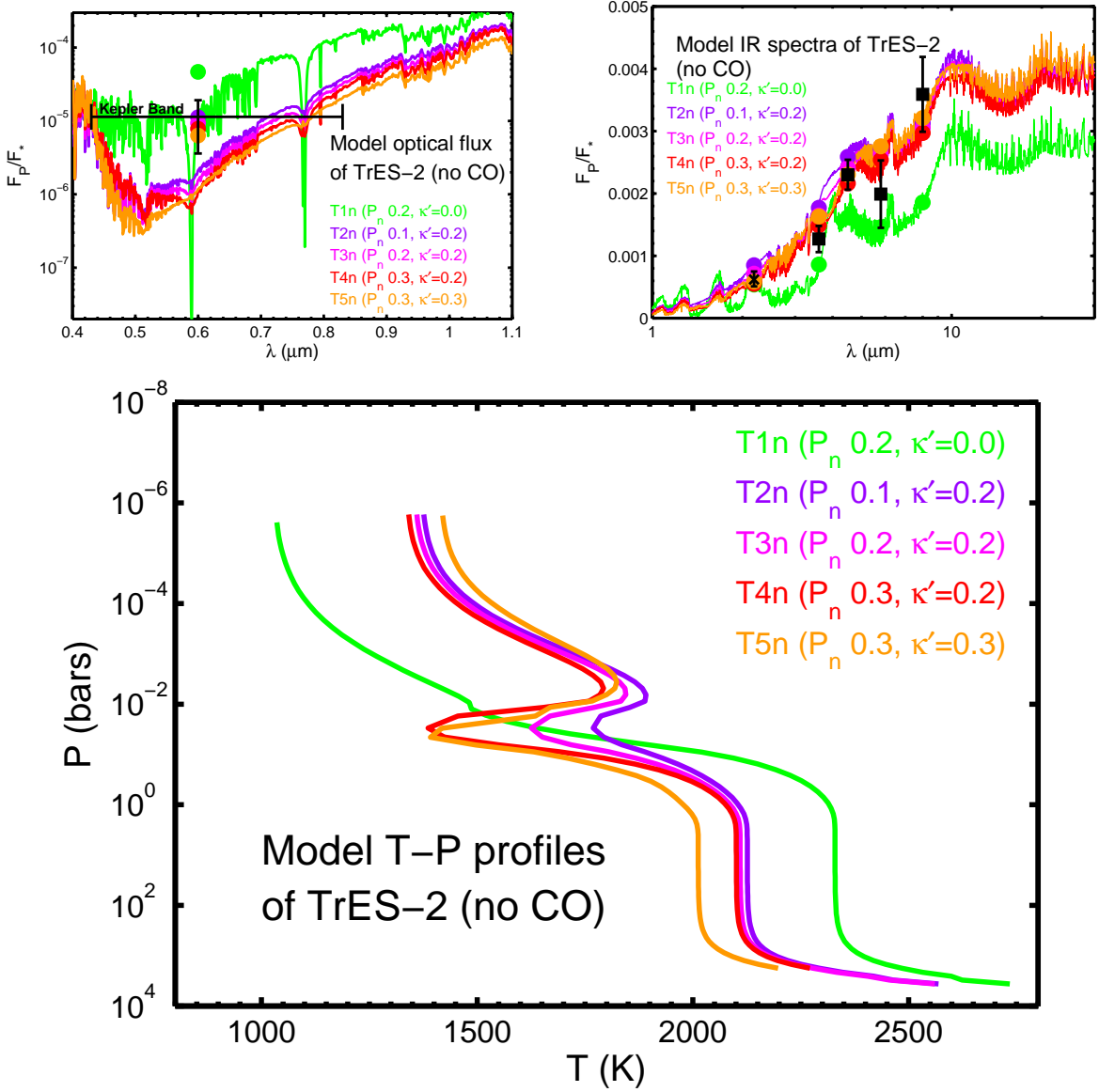


FIG. 3.— TrES-2 nonequilibrium chemistry model atmospheres, analogous to Fig. 2, but with CO artificially removed from the opacities and with  $\text{CH}_4$  and  $\text{H}_2\text{O}$  correspondingly enhanced. Below, we compare with the models shown in Fig. 2. *Top left:* Optical planet-star flux ratios, with Kipping & Bakos (2010) data (including  $2\text{-}\sigma$  error bars) shown. As in Fig. 2, models with upper atmosphere absorption (T2n–T5n) tend to have low optical flux ( $F_p/F_* \lesssim 2 \times 10^{-5}$ ). With  $\kappa' = 0 \text{ cm}^2 \text{ g}^{-1}$  (model T1n), the optical flux ratio is  $\sim 5 \times 10^{-5}$ , higher than the corresponding model in Fig. 2, but still low compared with the HAT-P-7b data and models. Models T2n–T5n are all consistent with the data, to  $2\sigma$ . *Top Right:* Infrared planet-star flux ratios. Again, the IRAC data clearly favor models with some extra absorption. The  $5.8\text{-}\mu\text{m}$ -discrepancy for model T5n is significantly reduced compared with the corresponding model with equilibrium chemistry. With CO removed, model T4n is a reasonably good fit to the data (within  $\sim 1\sigma$  at all IRAC bands). *Bottom:* Temperature-pressure profiles. The overall features of the profiles are similar, but the detailed shapes of the profiles are somewhat different, with isothermal regions  $\sim 100 \text{ K}$  warmer and upper atmospheres  $\sim 100 \text{ K}$  cooler than the equilibrium chemistry models.

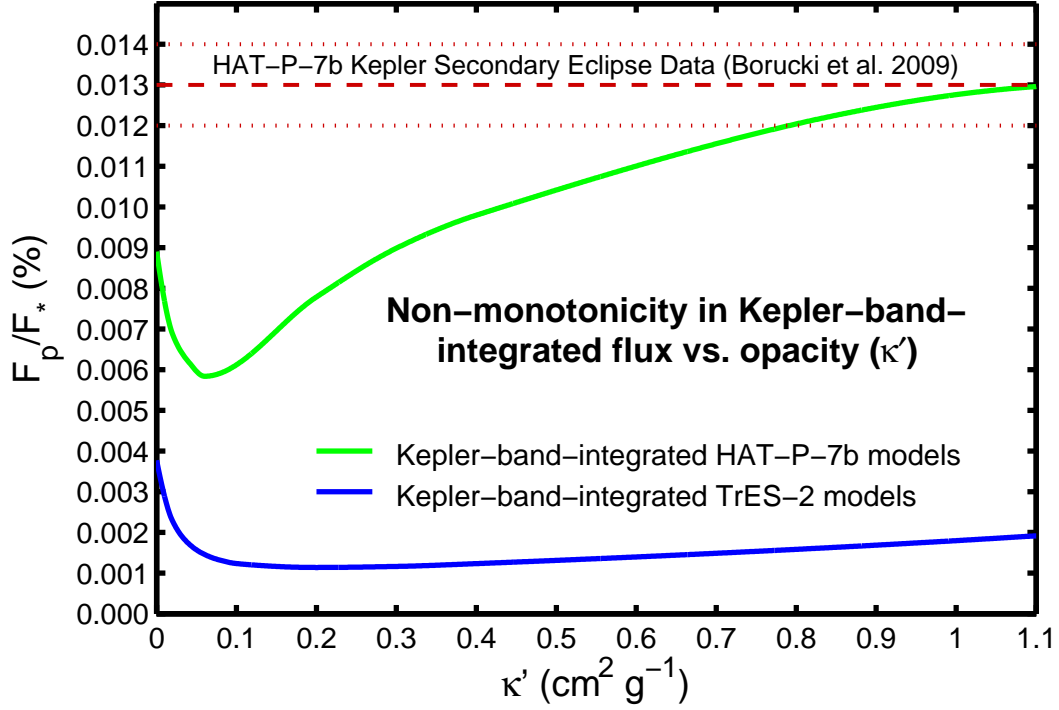


FIG. 4.— *Kepler* bandpass brightness ratios vs. upper atmosphere absorption ( $\kappa'$ ). Models of HAT-P-7b (thick light green) and TrES-2 (thick blue) are shown, in addition to the *Kepler* data for HAT-P-7b (dashed red) with  $1-\sigma$  errors (dotted dark green). These models have no redistribution to the nightside ( $P_n = 0$ ). The relationship between optical flux and  $\kappa'$  is non-monotonic for both planets, but more so for HAT-P-7b. In particular, for HAT-P-7b, large enough values of  $\kappa'$  (values above  $\sim 0.3 \text{ cm}^2 \text{ g}^{-1}$ ) lead to enough flux in the region of the Wien tail that the optical flux is greater than it would be with no extra absorber. However, for TrES-2, despite the non-monotonicity, the planet is still brightest in the optical without any extra absorber.